Article:
Gonçalves, M.C.C., Alsters, R., Curtis, D. et al. (2025) Analysis of tool wear in micromilling Ti6Al4V and its impact on generated surface integrity. Wear, 570. 205955. ISSN: 0043-1648

https://doi.org/10.1016/j.wear.2025.205955

Analysis of tool wear in micromilling Ti6Al4V and its impact on generated surface integrity

Maria Clara Coimbra Goncalves[a], Rob Alsters[b], David Curtis[c], Volodymyr Bushlya[d], Rachid M'Saoubi[d,e], Hassan Ghadbeigi[a]

[a]*University of Sheffield, Mechanical Engineering Department, Mappin Street, Sheffield, UK*
[b]*R&D Materials and Technology Development, Seco Tools AB, Zandterweg 14, Lottum, 5973 RC, Netherlands*
[c]*Advanced Manufacturing Research Centre, University of Sheffield, Rotherham, S60 5TZ, UK*
[d]*Lund University, Ole Römers väg 1, Lund, 221 00, Sweden*
[e]*R&D Materials and Technology Development, Seco Tools AB, Fagersta, 737 82, Sweden*

Abstract

Tool wear is one of the dominant factors that impacts the surface integrity of machined materials. Understanding the impact of tool wear on surface integrity is crucial in micromilling, due to the size of the features being machined and the cutting tools. Therefore, this work aims to analyse the impact of tool wear on surface integrity during the micromilling of Ti6Al4V. In this context, microslots were manufactured on a Ti6Al4V workpiece using both coated and uncoated 1 mm flat end mills at constant cutting parameters with varying cutting lengths in order to analyse the progression of tool wear with machined length and its impact on surface integrity. The microtools were investigated using both Scanning Electron Microscope (SEM) and infinite focus optical imaging (Alicona) to determine the tool wear evolution. Surface integrity was assessed by analysing surface roughness areal parameters, surface microscope images, and subsurface microstructure and microhardness perpendicular to the cutting direction. The results show that surface quality was not affected by the evolution of tool wear, with surface topography, including surface roughness parameters, remaining within a similar range until the catastrophic failure of the tool. Analysis of the machined surface revealed small chips adhered to it, which affected the surface texture height measurements, leading to a predominance of atypical peaks on the surface. Subsurface analysis of the machined material showed that the microstructure and microhardness remained consistent with the bulk material characteristics, indicating no evidence of severe plastic deformation in the machined subsurface. However, once the tool failed and began rubbing against the workpiece surface, swept grains due to material dragging and heat-affected zones were observed in the subsurface microstructure. Swept grains, caused by material extrusion, were also observed in the microstructure of the top burr formation regions throughout the experiments. From the tool wear morphology analyses, adhesive wear was the main wear mode observed, with abrasion, built-up edge formation and heat-affected zones also being observed in the tools.

Keywords: Micromilling, tool wear, titanium alloys, surface integrity, machining

1. Introduction

Micromilling is a manufacturing process based on mechanical material removal using micromills with a diameter ranging from 1 μm to 1 mm [1]. In recent years, many studies have highlighted the trend towards components miniaturisation [2, 3, 4], and micromilling is an efficient and precise method for manufacturing complex three-dimensional shapes in microscale. This process has enabled industries to develop precise features and components, such as microturbines, micromotors, micromoulds, microfluidic devices, and many others [1]. Despite its importance for the manufacturing sector, the application of micromilling in industry is limited by its inherent physical process challenges, as scale effects, process stability, and rapid tool wear [2, 5]. This has led to a growing emphasis on in-depth research into these underlying process mechanics [2, 4, 6, 7].

An important factor that affects part performance is the quality of the micromachined surface, which is commonly evaluated through the analysis of surface integrity metrics such as burr formation, surface defects, and subsurface microstructure [8, 9, 10]. In the context of analysing the machined subsurface, Meijer *et al.* (2022) [11] examined the micromilling process

as an approach to add compressive residual stresses to the workpiece subsurface in order to increase the component's service life. In the same area Platt *et al.* (2024) [12] has investigated the surface integrity during the micromilling of AISI H11 Tool Steel and observed minor changes in the subsurface microstructure during the micromilling process, but an increase in superficial microhardness and high compressive residual stresses on the material's surface, which can also be explored in terms of improving the components fatigue resistance.

Besides the importance of analysing the surface integrity of the machined part, analysing tool wear is another crucial aspect for better understanding the process mechanics and improving the micromachining process efficiency. In this context, Alhadeff *et al.* (2019) [3] proposed a protocol for analysing tool wear, describing a procedure for how to position and measure different wear types in a SEM. The same researchers concluded that the slot profile analyses did not provide much information on tool wear. In the same area, Gomes *et al.* (2021) [13] also proposed an approach to measure tool wear in micromilling. The authors used a SVM (Support Vector Machine) artificial intelligence model, based on vibration and sound signals, to monitor tool wear when micromilling AISI 316L. The authors also used the SEM to measure flank wear, and they established a wear measurement criterion of 13 µm as end of tool life, which was achieved at the machined length of 125 mm. Ziberov *et al.* (2020) [14] analysed the performance of two different coatings for micromilling Ti6Al4V alloy under dry and minimum quantity lubrication (MQL) conditions. For the conditions tested, the authors observed longer tool life for the dry micromachining condition when using a tool with diamond-like carbon (DLC) coating.

Even tough the literature provides valid information on how to analyse wear for certain tools, the limited reliable literature on tool wear in micromachining often analyse tool wear by measuring the worn length or analysing the reduction in tool diameter [3, 13, 15]. However, tool wear does not always follow a clear and easily measurable pattern in micromilling, and the small size of the tools further complicates this approach. Additionally, using other sensors to address tool wear increases both the complexity and cost of the analysis. Therefore, this paper adopts a different approach, also based on SEM images to analyse tool wear, but employs imaging processing techniques to quantitatively estimate tool wear, as previously reported in the analyses of conventional machining processes [16]. Hence, the goal of this paper is to analyse the progression of tool wear with machined length and its impact on the surface integrity of a rolled Ti6Al4V alloy. The surface integrity is assessed in this paper by analysing areal surface roughness parameters, surface topography, and subsurface microstructure and microhardness.

2. Methodology

The micromilling process was performed in a Kern Evo CNC centre. To perform the tests, the slot milling strategy was adopted and Ti6Al4V samples of 100x75x10 mm were mounted on a fixture (Figure 1) and slots of 75 mm length were manufactured following the design of experiments (DoE) presented in Table 1. This DoE was chosen in order to observe the microtools in different stages of tool wear. The remaining machining parameters were chosen based on recommended guidelines by the manufacturer for the condition, milling strategy, workpiece material and tool selected. These parameters were kept constant and they are detailed in Table 2.

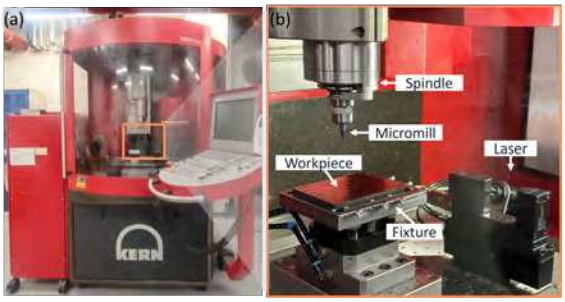

Figure 1: Setup of the micromilling tests performed.

Table 1: Design of experiments

Test	Tool #	Machined length [mm]
C1	Coated 1	1125
C2	Coated 2	2250
C3	Coated 3	Tool failure
U1	Uncoated 1	1125
U2	Uncoated 2	2250
U3	Uncoated 3	Tool failure

For each test performed, a new micromill was used. The microtools were solid carbide flat end mills with a diameter of 1 mm and two flutes, produced by SECO Tools. To assess the impact of the coating on the results, both uncoated and SIRON-A coated tools (code: JME562010G2R010.0Z2-SIRA) were utilized. The cutting edge radius, wedge angle, and nose radius of these tools were measured using an optical 3D measuring system (Alicona Infinite Focus). The average val-

Table 2: Constant parameters

Parameter	Value
Depth of cut (a_p)	300 µm
Cutting speed (V_c)	140 m/min (44600 rpm)
Feed (f_z)	15 µm/tooth (1340 mm/min)
Tool diameter	1 mm
Condition	dry cut
Strategy	slot milling
Workpiece material	Ti6Al4V

ues for these parameters, calculated from eight measurements, are shown in Table 3. To standardise inaccuracies and vibrations caused by tool bending during cutting, the tools were clamped to the tool holders maintaining the same distance from the collet to the tip of the tool. After mounting the entire assembly on the spindle, their quasi-static tool run-out was measured using a dial indicator mounted on a magnetic base. The tool run-out was maintained below 1 µm for all tools, and they were kept in their respective tool holders until the completion of the tests.

Table 3: Tools measurements

Parameter	Uncoated tool	Coated tool
Cutting edge radius [µm]	5.72 ± 0.43	8.70 ± 0.62
Wedge angle [°]	70.18 ± 2.34	71.20 ± 4.28
Nose radius [µm]	88.09 ± 2.16	85.34 ± 6.01

Before performing the experiments, the rolled Ti6Al4V Grade 5 workpiece underwent a stress relief heat treatment to improve the stability of the material properties and eliminate residual stresses. The heat treatment consisted of heating the material to 600°C for 3 hours, followed by furnace cooling. The workpiece's microstructure is shown in Figure 2, where a typical bimodal microstructure of the rolled Ti6Al4V can be observed. The microstructure consists of α-phase (darker regions) in form of equiaxed grains, β phase (brighter regions) in a lower volume fraction, and a lath-structure of α and β plates [17]. The hardness of the bulk material was measured to be 346.8 ± 42.4 HK0.2 averaged out of five measurements.

To analyse the slots subsurface after the micromilling experiments, the workpiece was cut perpendicular to the cutting direction and mounted in bakelite for grinding and polishing. After that, the microhardness was also measured on the slots subsurface using the Vickers and Knoop methods. Six measurement points were taken along the machined subsurface of a randomly selected experiment to observe how the hardness varies

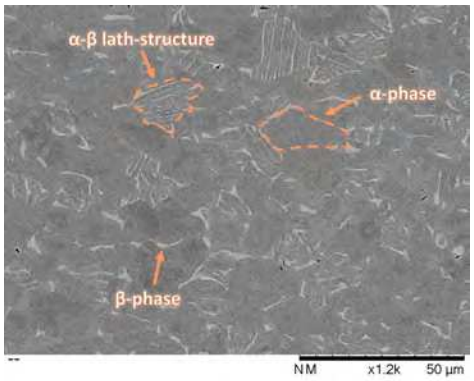

Figure 2: Ti6Al4V workpiece microstructure.

in the machined subsurface and to compare it with the bulk material hardness. The tool wear was assessed by analysing the top view of the tools in a SEM Hitachi TM3030 plus, as well as the cutting edge views in an Alicona Infinite Focus. The SEM images acquired were processed in the ImageJ software by using a find edge filter to highlight the sharp changes in intensity within the images. By doing that, the new and worn tools gradually differentiate in the amount of white pixels and mean grey value, which allows for a quantitative comparison of the tool wear.

3. Results and discussion

3.1. Surface topography evaluation

The topography of the machined slots was evaluated by analysing its height surface texture parameters [18] and its two-dimensional images obtained in Alicona. The surface roughness results for the S_a parameter (arithmetic mean height) can be seen in in Figure 3, where the results can be seen separately for each tool (Figure 3(a)) and as a comparison between the coated and uncoated tools (Figure 3(b)).

Figure 3 shows that there was no significant change in the S_a results due to tool wear up until the point that the tool broke and started rubbing against the surface, which caused the S_a values to increase to up to 3 µm. Similarly, the use of a coating had no significant impact on surface roughness in the applied machining parameters. Excluding the tool failure point, the average S_a value was 0.27 ± 0.05 µm for the coated tools and 0.25 ± 0.05 µm for the uncoated tools, indicating that tool coating results were essentially the same for both tool types. Although there was no significant change in the surface roughness for either the coated or uncoated tool up until the breakage point, the coated tool presented

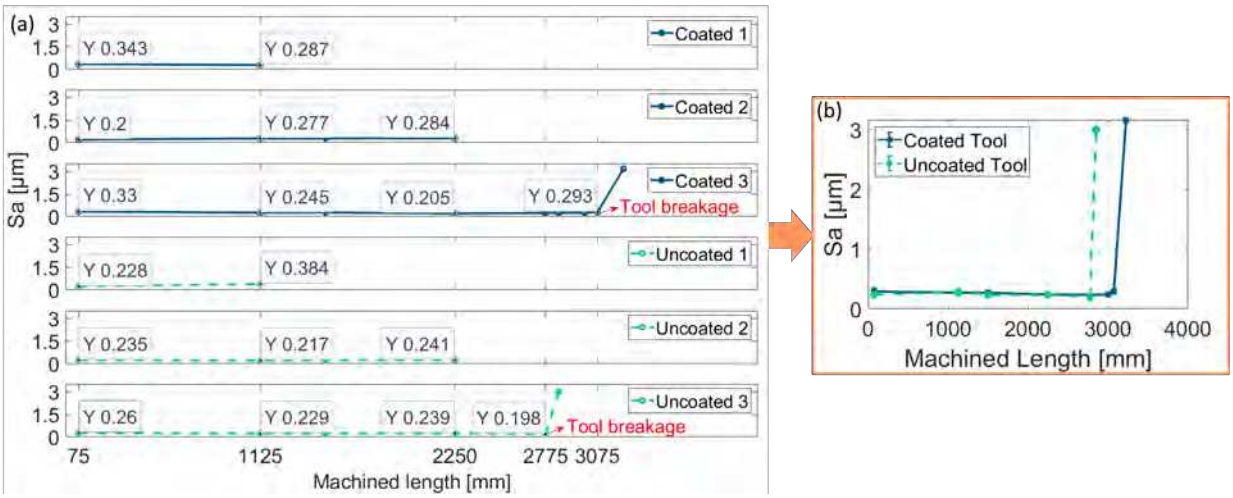

Figure 3: Sa results for each experiment performed and as a comparison of the coated and uncoated tools per machined length.

a longer tool life, reaching its failure at 3075 mm machined, while the uncoated tool broke at 2775 mm machined.

The same trend can be observed for the other parameters that characterise surface amplitude, such as S_q, S_p, S_v, and S_z, as shown in Figure 4. Since S_p, S_v, and S_z represent the maximum peak height, maximum valley depth and their sum [19], respectively, chips attached to the machined surface influence these measurements, particularly S_p and S_z, which explains the greater variation in these results. The Skewness (S_{sk}) and Kurtosis (S_{ku}) characterise the shape of the height distribution [19]. The positive results obtained for the S_{sk} values indicate that the height distribution is skewed above the mean plane [18], effectively meaning that the surface has a predominance of peaks. The S_{ku} values were greater than three for all measurements made, implying that the distribution contains atypical peaks on the surface [18], which, again, is influenced by random chips attached to the surface, even after cleaning.

By analysing the two-dimensional images of the slots obtained in Alicona (Figure 5) it is possible to observe some small chips attached to the machined surface, and Figure 5 also shows that, as the machined length increases, the feed marks on the surface becomes slightly more asymmetrical due to tool wear. In addition, the feed mark spacing behaves as expected, at around 15 µm, matching the feed per tooth used (Figure 5).

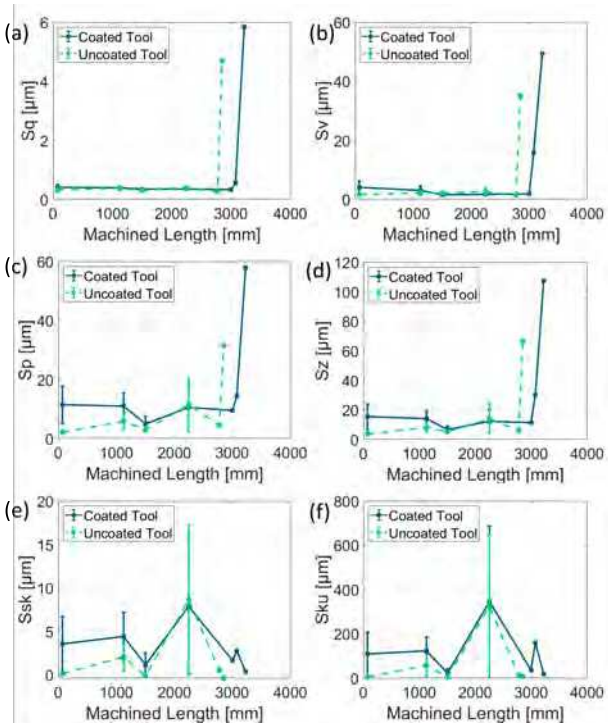

Figure 4: Comparison of areal height surface texture parameters per machined length for the coated and uncoated tools.

3.2. Subsurface analysis

To analyse the slots subsurface, the workpiece was cut perpendicular to the cutting direction and mounted in bakelite for grinding and polishing. Even without etching, it is possible to use a SEM to visualise

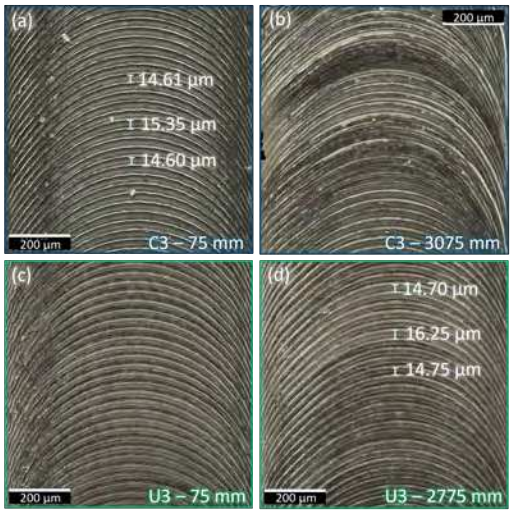

Figure 5: Comparison of the slot surfaces at a low machined length and before the tool failure.

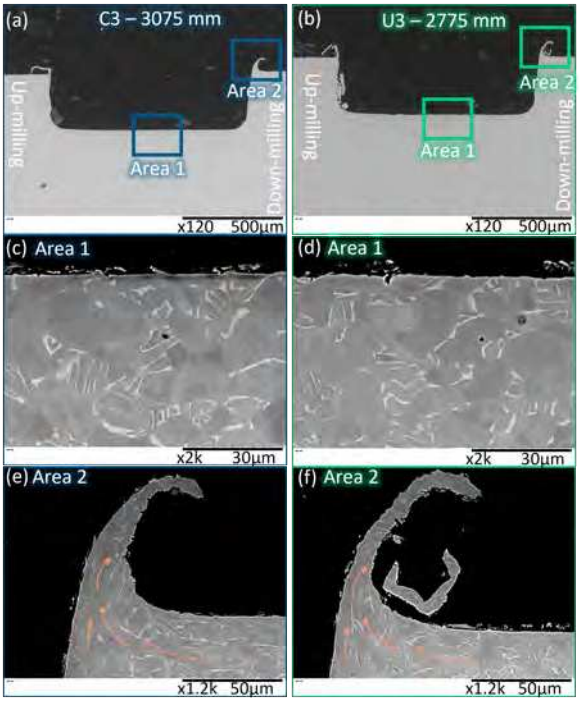

Figure 6: Subsurface evaluation for the coated and uncoated tools before failure.

the workpiece microstructure by adjusting the imaging brightness and contrast, as shown in Figure 6. This figure presents the slot profile for both coated and uncoated tools near tool failure (Figures 6(a) and 6(b)) with highlights at the regions that were zoomed in for microstructure analyses. It is possible to see from Figures 6(c) and 6(d) that the microstructure on the bottom machined surface did not significantly differ from the bulk material (shown in Figure 2), even near tool failure. This suggests that, despite the shearing process inherently involving material dragging and plastic deformation, no signs of material dragging or plastic deformation were observed in the bottom slot subsurface microstructure. In contrast, the microstructure at the top burr shows grains distorted outward, as highlighted by the orange arrows in Figures 6(e) and 6(f), which is caused by the material near the interface being pushed or extruded away.

From the surface analyses presented in Section 3.1, it was possible to observe that the tool breakage occurs abruptly. The tool breakage point was particularly evident in the U3 test, as shown in Figure 7, where the top and side views of the slots are compared near tool failure and after it. Unlike what was observed in the microslot subsurface, when the broken tool rubs against the surface, the workpiece material experiences severe plastic deformation, with the formation of a heat affected zone (HAZ) and deformed grains below it (Figure 8). This deformation occurs because the friction between the broken tool and the workpiece generates significant heat, and without proper shearing, this heat leads to extensive material deformation.

The microhardness results are presented in Figure 9. All hardness measurements were performed on the U3 experiment at the machined length of 2775 mm. The heatmap in Figure 9(a) shows the microhardness variation along the slot using a colour scale, based on the measurement points (p1–p6 in the figure) from the Vickers hardness test. The Knoop method was also applied for measuring the hardness in the slot profile, and its results can be seen in Figure 9(b). In Figure 9(b), the orange lines depict the variation in Knoop hardness of the bulk material, with the average of 346.8 ± 42.4 HK0.2 out of five measurements. It can be observed that hardness measurements from the subsurface were similar to those of the bulk material, reflecting their similar microstructures. Since no plastic deformation was observed in the slot subsurface due to the shearing process, it is expected that the hardness of the slot subsurface would be similar to that of the bulk material. The high standard deviation between measurements, observed consistently in both the bulk and slot subsurface, can be attributed to the variations in grain orientation and phase distribution within the material. This variability in hardness measurements is expected in the Ti6Al4V alloy, as it is an α-β alloy with differences in the crystal structures of each phase. Consequently,

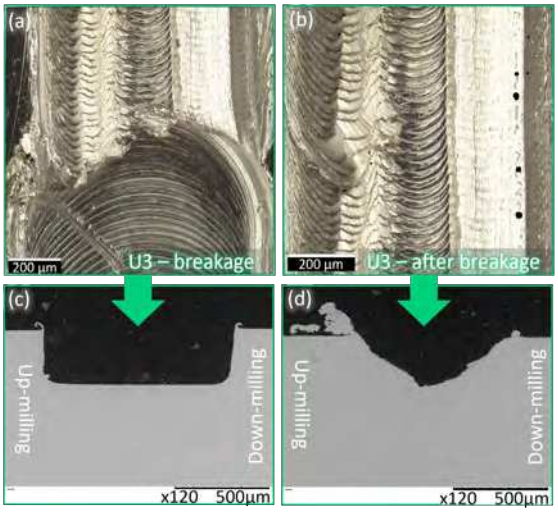

Figure 7: Top and side views of the slots for test U3 near and after tool catastrophic failure.

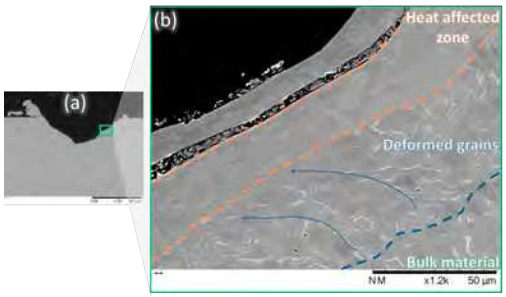

Figure 8: Subsurface microstructure of the broken slot for test U3.

hardness values may vary depending on the specific location of the measurement.

3.3. Tool wear analysis

Figures 10 and 11 show the SEM images acquired for the coated and uncoated tools, respectively, and their corresponding filtered images with their white pixel percentage and mean grey value results. All conditions during SEM image acquisition were kept the same for all images, which allows for a comparison between the tools.

From Figures 10 and 11, the first evident observation is that the white pixel percentage is higher for the uncoated tool. This is due to changes in the reflection properties of the tool material without the coating. For this reason, the results can be compared between tools under the same coating conditions. When analysing the coated and uncoated tools separately, it is possible to observe that both the white pixel percentage and the mean grey value increase with tool wear in both cases, pri-

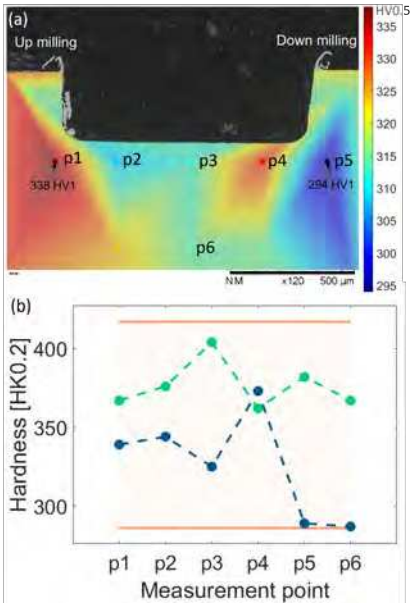

Figure 9: Subsurface hardness measurements results: (a) Vickers hardness map including measumerents points 1 to 6; and (b) Knoop results for measumerents points 1 to 6.

marily due to material adhesion on the relief face and gash of the tool. Although image processing reveals this difference, it is difficult to visually detect from the top view of the tools or to easily measure tool wear, as is commonly approached in literature [3, 6, 14]. This makes it challenging to detect the gradual deterioration of the tool due to wear before its catastrophic failure, which occurs shortly after machining 2250 mm under the tested conditions.

Detailed analysis of these tools in the flank face view are presented in Figures 12 and 13, showing an EDS of the cutting edge region, for the coated and uncoated tools, respectively. From the SEM images shown in Figures 12 (a), (b) and (c) it can be seen that Ti6Al4V chips and microchips are adhered along the coated tool. Also, there is a lack of coating in the edge of the tool, confirmed by the detection of the cemented carbide components (tungsten and cobalt) in the cutting edge from the EDS analysis presented in Figure 12 (d). Morever, Figure 12 (d) shows the tool coating in red, made from Chromium and Aluminum, and adhered Ti6Al4V throughout. Similarly, Figures 13 (a), (b) and (c) show an worn uncoated tool edge near failure, where adhered material and abrasion can be observed. Figure 13 (d) presents the EDS analysis of the region near the cutting edge showing the Ti6AlV material elements adhered to the cemented carbide tool. From these images, it can be seen that adhesive wear is predominant in both

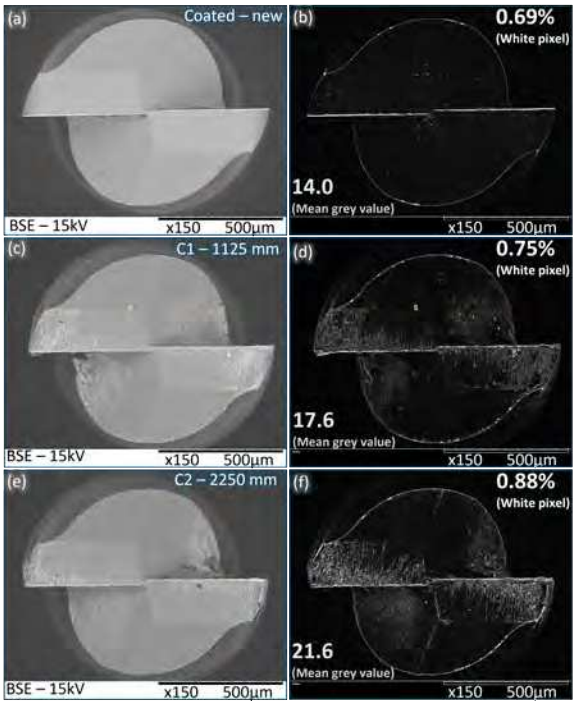

Figure 10: SEM images of the coated tools in different stages of machined length.

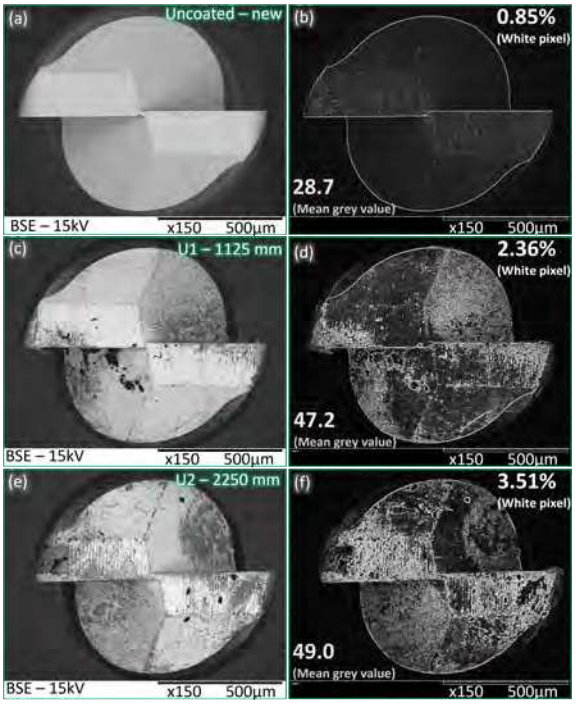

Figure 11: SEM images of the uncoated tools in different stages of machined length.

tools, which can be addressed to a poor thermal diffusion in the tool-chip-workpiece interface. Additionally, besides material adhesion specially in the cutting edge and flank, the cutting edges of both tools did not present signs of severe degradation before its breakage point.

Another view of the tools is provided in Figures 14 and 15, which present the rake and flank face images of the coated and uncoated tools at different machined lengths, respectively. From the flank face view shown in Figures 14(b), 14(d), 15(b), and 15(d), it can be seen how the Ti6Al4V material smearing over the flank increases with the machined length. Besides that, HAZ and built-up edge formation were also observed on the tools, as indicated in Figures 14 and 15. When closely analysing the top view of the tools in the SEM (Figure 16), the sliding material over the flank can be observed, as indicated in the figure. The formation of BUE on the tool's cutting edge and chip formation on the primary relief face of the tool can also be observed by the perspective presented in Figure 16.

The presence of the tool wear modes observed weakens the tool tip, contributing to its catastrophic failure. Another factor that can also influence the abrupt breakage is the complexity of the material flow in the microscale, which can cause the tool to get stuck and break unexpectedly, as shown in Figure 7(a). The complexity of material flow is seen by the chip formation and material adhesion observed not only on the tool flute, but also on the relief face and gash of the tool (Figures 10, 11, and 16). These factors collectively contribute to the tool's catastrophic failure. As the tool wears, the complexity of material flow behaviour worsens due to material diffusion, which in turn increases the cutting loads, ultimately resulting in mechanical failure of the tool at a macro level. In this situation, the influence of the coating is less significant, as the tool breakage is more related to the tool geometry, which directly affects the material flow, rather than the tool coating itself.

4. Conclusions

This paper focused on analysing the impact of tool wear on the machined surface during the micromilling process of Ti6Al4V. In this context, surface topography, subsurface characteristics, and tool wear results were compared when using coated and uncoated tools. The key findings of this paper, considering the specific set of parameters employed, are as follows:

- Tool wear did not significantly impact surface roughness measurements up until the tool breakage point, when the tool begins rubbing against

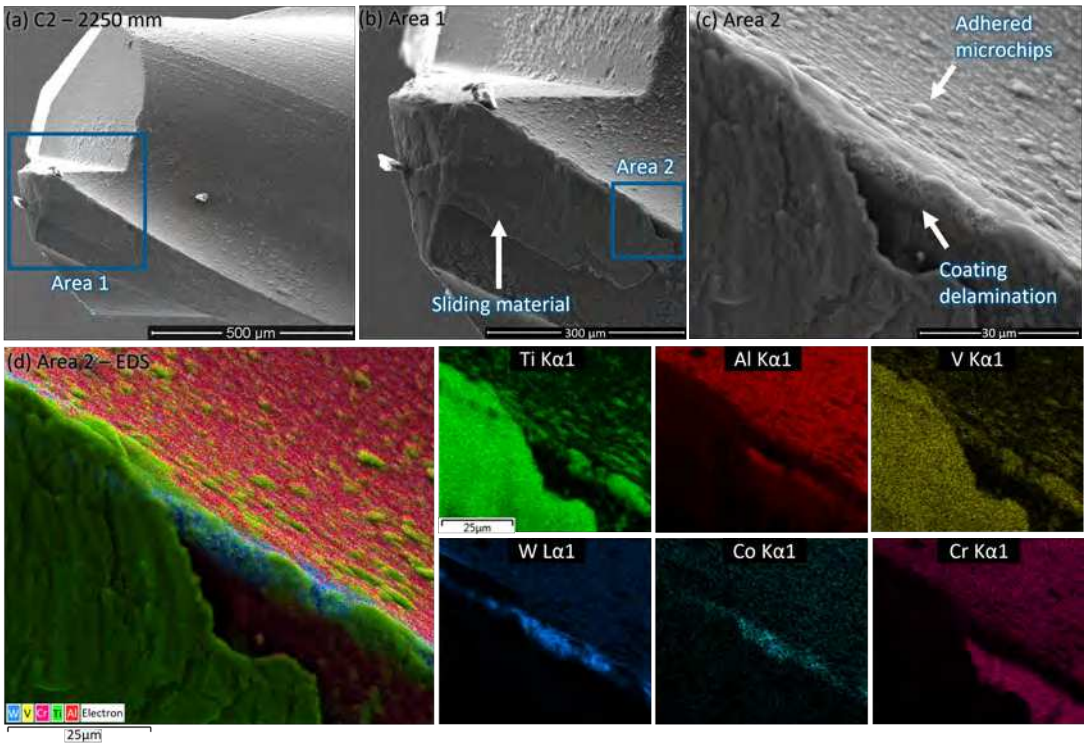

Figure 12: SEM images and EDS analysis of a coated tool tip at the machined length of 2250 mm.

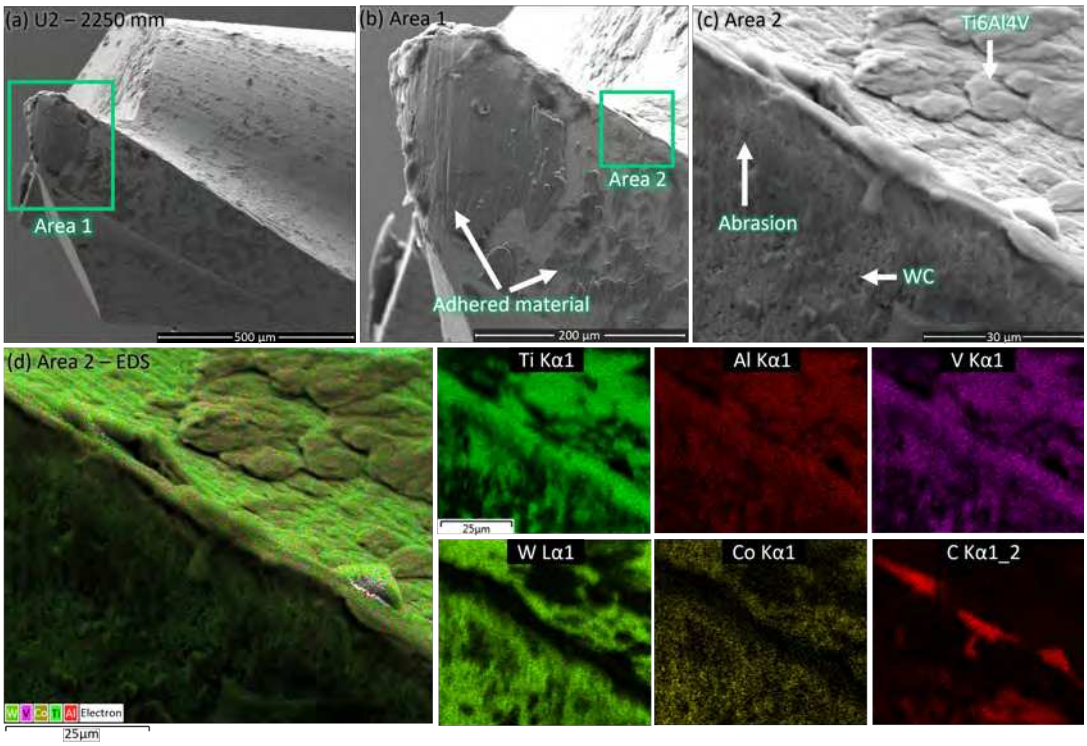

Figure 13: SEM images and EDS analysis of an uncoated tool tip at the machined length of 2250 mm.

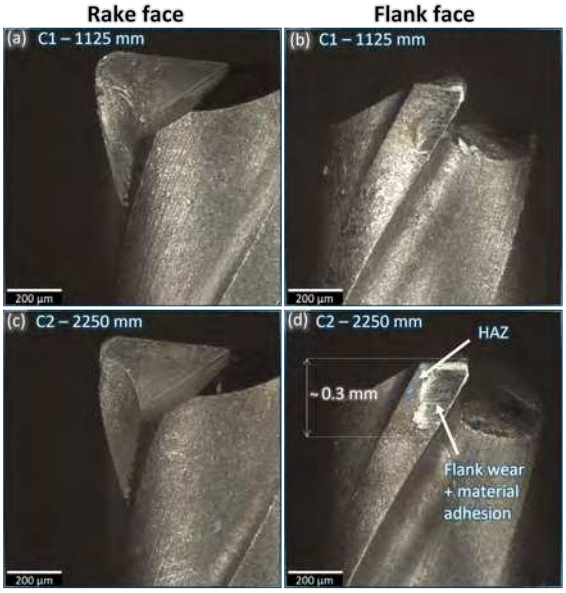

Figure 14: Rake and flank face of the coated tools in different stages of machined length.

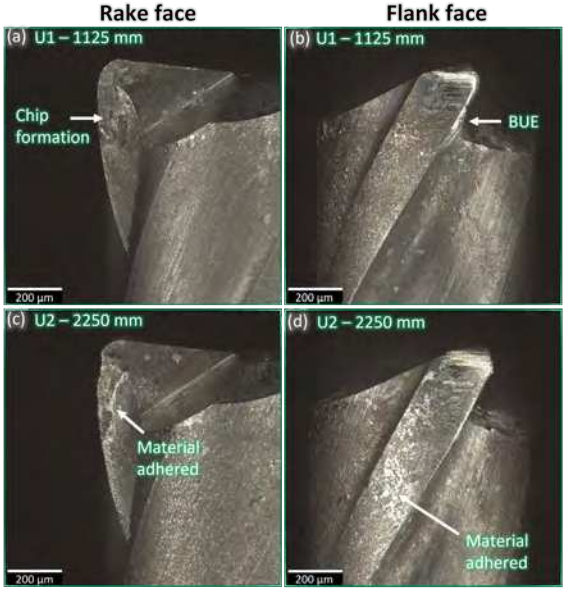

Figure 15: Rake and flank face of the uncoated tools in different stages of machined length.

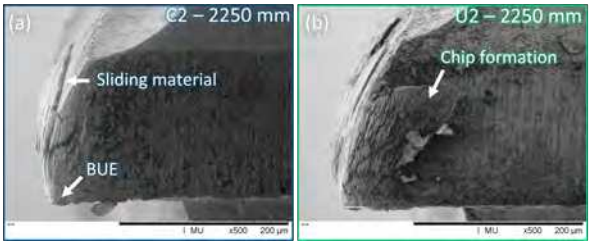

Figure 16: Close-up view of the tool tips for both coated and uncoated tools at a machined length of 2250 mm.

the workpiece material. At this stage, the friction generates significant heat, leading to material plastic deformation with HAZ formation and deformed grains underneath the surface;

- The average S_a values of the machined surfaces were 0.27 ± 0.05 µm and 0.25 ± 0.05 µm for the coated and uncoated tools, respectively, indicating that the S_a results did not vary with tool coating;
- The machined surface presented a predominance of atypical peaks, which is due to random chips attached to the surface that influence the shape of the height distribution;
- The microstructure on the bottom slot subsurface did not significantly differ from the bulk material. However, the microstructure at the top burr shows grains distorted outward, resulting from the plastic deformation of the material near the interface being pushed or extruded away;
- The microhardness measurements on the machined subsurface exhibited similar behaviour to the bulk material, with wide hardness variations influenced by the sample's microstructure;
- Tool breakage happens abruptly due to a combination of tool wear and the complex material flow, which can cause the tool to get stuck and break. This suggests that, at this scale, tool geometry has a greater impact on tool failure than tool coating, as geometry directly affects material flow;
- Adhesive wear was the dominant wear mode observed in the experiments performed. However, material abrasion, HAZ, and built-up edge formation were also present during tool analysis.

Acknowledgements

This study was conducted under the grants of the Engineering and Physical Sciences Research Council (EPSRC) Doctoral Training Partnership Case Conversion

with Seco Tools (grant number: EP/W524360/1). Additionally, the authors would like to thank Dr. Matthew Brown from the AMRC for their guidance throughout the research development.

References

[1] M. A. Câmara, J. C. Campos Rubio, A. M. Abrão, and J. P. Davim. State of the art on micromilling of materials, a review. *Journal of Materials Science & Technology*, 28(8):673–685, 2012.

[2] L. O'Toole, C. Kang, and F. Fang. Precision micro-milling process: state of the art. *Advances in manufacturing*, 9:173–205, 2021.

[3] L. L. Alhadeff, M. B. Marshall, D. Curtis, and T. Slatter. Protocol for tool wear measurement in micro-milling. *Wear*, 420: 54–67, 2019.

[4] E. Kuram and B. Ozcelik. Optimization of machining parameters during micro-milling of Ti6Al4V titanium alloy and Inconel 718 materials using Taguchi method. *Proceedings of the Institution of Mechanical Engineers, Part B: Journal of Engineering Manufacture*, 231(2):228–242, 2017.

[5] K. Aslantas, H. E. Hopa, M. Percin, İ. Ucun, and A. Çicek. Cutting performance of nano-crystalline diamond (NCD) coating in micro-milling of Ti6Al4V alloy. *Precision Engineering*, 45:55–66, 2016. doi: https://doi.org/10.1016/j.precisioneng.2016.01.009.

[6] M. C. Gomes, A. G. Santos, D. Oliveira, G. V. Figueiredo, K. S. B. Ribeiro, G. A. B. Rios, M. B. Silva, R. T. Coelho, and W. N. Hung. Micro-machining of additively manufactured metals: a review. *The International Journal of Advanced Manufacturing Technology*, pages 1–20, 2022.

[7] M. C. C. Gonçalves, R. Alsters, D. Curtis, R. M'Saoubi, and H. Ghadbeigi. Evolution of surface quality in micromilling Ti-6Al-4V alloy with increasing machined length. *Procedia CIRP*, 123:221–226, 2024.

[8] S. Dehen, E. Segebade, M. Gerstenmeyer, F. Zanger, and V. Schulze. Milling parameter and tool wear dependent surface quality in micro-milling of brass. *Procedia CIRP*, 87:95–100, 2020. ISSN 2212-8271. doi: https://doi.org/10.1016/j.procir.2020.02.024. 5th CIRP Conference on Surface Integrity (CSI 2020).

[9] B. Z. Balázs and M. Takács. Experimental investigation of the influence of cutting parameters on surface quality and on the special characteristics of micro-milled surfaces of hardened steels. *Proceedings of the Institution of Mechanical Engineers, Part C: Journal of Mechanical Engineering Science*, 235(23): 6996–7008, 2021. doi: 10.1177/09544062211013064.

[10] L. Chen, D. Deng, G. Pi, X. Huang, and W. Zhou. Burr formation and surface roughness characteristics in micro-milling of microchannels. *The International Journal of Advanced Manufacturing Technology*, 111:1277–1290, 2020.

[11] A. L. Meijer, D. Stangier, W. Tillmann, and D. Biermann. Induction of residual compressive stresses in the sub-surface by the adjustment of the micromilling process and the tool´s cutting edge. *CIRP Annals*, 71(1):97–100, 2022. ISSN 0007-8506. doi: https://doi.org/10.1016/j.cirp.2022.04.065.

[12] T. Platt, A. L. Meijer, and D. Biermann. Experimental Investigation on the Surface Integrity in Micromilling AISI H11 Tool Steel. *Procedia CIRP*, 123:65–70, 2024. ISSN 2212-8271. doi: https://doi.org/10.1016/j.procir.2024.05.014. 7th CIRP Conference on Surface Integrity.

[13] M. C. Gomes, L. C. Brito, M. B. Silva, and M. A. V. Duarte. Tool wear monitoring in micromilling using support vector machine with vibration and sound sensors. *Precision Engineering*, 67:137–151, 2021. doi: https://doi.org/10.1016/j.precisioneng.2020.09.025.

[14] M. Ziberov, D. Oliveira, M. B. Silva, and W. N. P. Hung. Wear of TiAlN and DLC coated microtools in micromilling of Ti-6Al-4V alloy. *Journal of Manufacturing Processes*, 56:337–349, 2020. doi: https://doi.org/10.1016/j.jmapro.2020.04.082.

[15] R. Yadav, M. Kumar, N.D. Chakladar, A.M. Sidpara, and S. Paul. Evaluation of tool wear during micro-milling of ultrasonically assisted abrasive peened Ti-6Al-4V. *Wear*, 552-553, 2024. doi: https://doi.org/10.1016/j.wear.2024.205450.

[16] D. Y. Pimenov, L. R. R. Silva, A. Ercetin, O. Der, T. Mikolajczyk, and K. Giasin. State-of-the-art review of applications of image processing techniques for tool condition monitoring on conventional machining processes. *The International Journal of Advanced Manufacturing Technology*, 130(1):57–85, 2024.

[17] S. Vogel, D. Bhattacharyya, G. B. Viswanathan, D. Williams, and H. L. Fraser. Phase transformation textures in Ti6Al4V alloy. *Materials Science Forum*, 495-497:681–686, 09 2005. doi: 10.4028/www.scientific.net/MSF.495-497.681.

[18] ISO 25178-2:2021 (en). Geometrical product specifications (GPS) — Surface texture: Areal — Part 2: Terms, definitions and surface texture parameters. Standard, International Organization for Standardization, Committee ISO/TC 213, 2021.

[19] P. Pawlus, R. Reizer, and M. Wieczorowski. Functional importance of surface texture parameters. *Materials*, 14, 2021. doi: 10.3390/ma14185326.